Surface-Bound Gradient Deposition of Protein Nanoparticles for Cell Motility Studies

Witold I. Tatkiewicz,[1,2] Joaquin Seras-Franzoso,[2,3,4†] Elena Garcia-Fruitós,[2,3,4&] Esther Vazquez,[2,3,4] A. R. Kyvik,[1,2] Judith Guasch,[1,2,5] Antonio Villaverde,[2,3,4] Jaume Veciana[1,2*] and Imma Ratera[1,2*]

[1]Department of Molecular Nanoscience and Organic Materials, Institut de Ciència de Materials de Barcelona (CSIC), Campus UAB, 08193 Bellaterra (Spain)

[2]CIBER de Bioingeniería, Biomateriales y Nanomedicina (CIBER-BBN), 08193 Bellaterra (Spain)

[3]Institut de Biotecnologia i de Biomedicina (IBB), Universitat Autònoma de Barcelona, 08193 Bellaterra (Spain)

[4]Departament de Genètica i de Microbiologia, Universitat Autònoma de Barcelona, 08193 Bellaterra (Spain)

[5]Dynamic Biomaterials for Cancer Immunotherapy, Max Planck Partner Group, ICMAB-CSIC, Campus UAB, 08193 Bellaterra (Spain)

[†]Present address: Cibbim-Nanomedicine, Hospital Vall d'Hebron, Passeig de la Vall d'Hebron, 119-129, 08035, Barcelona, Spain

&Present address: Department of Ruminant Production, Institut de Recerca i Tecnologia

Agroalimentàries (IRTA), 08140 Caldes de Montbui, Spain.

Corresponding author: iratera@icmab.es

ABSTRACT. A versatile evaporation-assisted methodology based on the coffee-drop effect is

described to deposit nanoparticles on surfaces, obtaining for the first time patterned gradients of

protein nanoparticles (pNPs) by using a simple hand-made device. Fully customizable patterns

with specific periodicities consisting of stripes with different widths, heights and with distinct

nanoparticle concentration gradients can be produced over large areas (~10 cm^2) in a fast (up to 1

mm/min), reproducible, and cost-effective manner using an operational protocol optimized by an

evolutionary algorithm. The developed method opens the possibility to decorate surfaces "a-la-

carte" with pNPs enabling different categories of high throughput studies on cell motility.

INTRODUCTION

Bacterial inclusion bodies (IBs) are solid protein nanoparticles (pNPs), ranging from ca. 50 to

500-600 nm, which are non-toxic and mechanically stable.[1-4] They are functional amyloids that

are under exploration as drug delivery systems and as biochemical and topographical modifiers of surfaces at nano- and microscales for cell-guiding studies.[5-9] We have previously used these materials for surface decoration with geometrical patterns at constant pNPs concentrations for cell guidance.[10] Nevertheless, to the best of our knowledge, they have not been yet used to produce surface-bound gradients of pNPs like bacterial IBs.

Cells accommodate to their external environment and therefore to various external stimuli such as ramps of soluble biomolecules and gradients of topography or stiffness by moving to their preferred conditions.[11-12] Reproducing these gradients *in vitro* is one of the most popular and effective approaches to study cell motility.[13-16] To this end, few structures containing metallic (Au, Ag, etc.) and polymeric NPs have been reported, which include stripes, rings, grids, and dot-arrays.[17-23] Moreover, these structures are interesting for many other applications, ranging from transparent conductive electrodes[24-25] to plasmonic sensing materials.[26]

Although general methodologies for the generation of surface-bound gradients from soluble biomolecular factors have already been described,[27] there are only scarce examples of surface-bound particle gradients from colloidal suspensions.[28-29] Such examples use micellar solutions and the dip-coating technique and, as far as we know, there is no straightforward technique that allows obtaining surface-bound protein particle gradients from their colloidal suspensions. One way to tackle this shortcoming is the emerging field of evaporation-assisted deposition methods, based on the widely known "coffee-drop effect", named after the daily observation of stains left by colloidal coffee drops on plane surfaces.[17, 30] After drying, a characteristic deposit with a darker rim and a clear center can be observed, as opposed to homogenous depositions, in which an even layer of the deposited material is formed. The rim of the drop defines the area of particle self-assembly and can be referred as "contact line", "pinning line" or the "three-phase line". The

latter is to highlight the coexistence of a gas phase that enables evaporation, a liquid phase that evaporates, and a solid substrate where the particulate material is self-assembled.[31]

Recently, the field of evaporation-driven self-assembly resulted in a few original applications, such as the template-directed colloidal self-assembly technique.[32-33] In this approach, a colloidal suspension evaporates on a substrate with a previously modified topography, where grooves and pits guide the particles to the desired positions, as the drying front crosses these cues. Alternatively, microgrid masks, set above the substrate, were used as a template to control solvent evaporation, in a process denominated "confined dewetting lithography" or "evaporative lithography".[34-35] In this case, no topological or chemical pre-modification of the substrate was needed in order to deposit regular patterns on flat substrates. Another approach is based on the introduction of a chemical pattern onto the surface.[36-38] Predefined by microcontact printing, hydrophobic self-assembled molecular monolayer patterns were reported to guide the deposition of colloids, as these areas directed the pinning and the dewetting phenomena. Very complex forms with single particle resolution were also reported using a similar method[39] and nanowires produced from metallic quantum dots were obtained by "flow coating".[40] More interesting, control over distances of patterned stripes was demonstrated by an externally governed liquid level.[41] Specifically, fine-tuning of the velocity of the colloidal suspension "contact line" over the substrate to be functionalized was achieved with a computer-controlled syringe pump, having a direct impact on the geometry of the deposited patterns. This technique, referred as "convective self-assembly with liquid-level manipulation" (CSA-LLM), enables governing the deposit geometry in a template-free manner. CSA-LLM was successfully used to fabricate stripe, grid, and triangle patterns of AuNPs with specific periodicity, through controlling macroscopic experimental parameters, such as particle concentration of the colloidal suspension and

temperature.[42-43] Also, hybrid grids using first silica and then AgNPs were obtained and studied.[44] Another example consisted in the deposition of self-assembled "dotted lines" composed of AuNP clusters.[45] Moreover, CSA-LLM was applied to deposit stripes from aqueous suspensions of commercially available NPs (silica, Au, Ag) of a range of sizes between 10 and 270 nm on glass and polymer (PS, PET) substrates.[42-46] Recently, this technique was also adapted to pattern thermoactive microgel stripes on substrates to spatially control the cell adhesion and detachment.[46]

In spite of all these advancements, there are no reported examples of using similar approaches to pattern surface-bound gradients of pNPs, which have enormous advantages in comparison with conventional engineered inorganic NPs, like silica, Au, Ag, etc. These pNPs can be obtained by biotechnological procedures "a-la-carte" with a wide range of sizes, stiffness, and chemical and biological cues.[47] Here we present a new methodology to fill the above-mentioned gap and obtain concentration gradients of pNPs, on surfaces for cell guidance studies in a reproducible, simple, and cost-effective way.

MATERIALS AND METHODS

Preparation and characterization of IB colloidal suspensions. Production and purification of GFP-derived IBs was performed as previously described.[10] All prepared IB aliquots were re-suspended in MilliQ water. The resulting suspensions were sonicated for 10 minutes and left for 48 hours at 4 ºC. After that time, the suspension was harvested avoiding the sediment consisting of large particle aggregates. The working suspensions were obtained from the storage suspension by diluting it in MilliQ water to reach the desired particle concentration. Prior to the first use, the

working solutions were sonicated and purged for 10 minutes with argon for degasification. These IB solutions were examined by dynamic light scattering (Zetasizer Nanoseries, Malvern Instruments) and nanoparticle tracking analysis (LM20 unit, Malvern Instruments) to quantify the size (ranging from around 50 nm to a few hundred nanometers in diameter) and concentration of particles (240 µg ml^{-1} or otherwise stated) respectively.

Custom-made device for surface-bound gradient deposition of pNPs from colloidal suspensions. We designed the device (Figure 1) in order to (*i*) maximize the patterned area and (*ii*) minimize the volume needed of the working suspensions (ca. 10 ml). To fulfil both requirements a rectangular deposition cuvette with a very narrow cross-section was used. The device consists of two planar polystyrene plates separated by a custom U-shaped PDMS seal that are attached by elastic rubber bands to a rectangular metal reservoir which is used to stabilize and fix the device temperature. When compressed, the polystyrene plates and a U-shaped PDMS seal together forming a water-tight vessel that is large enough for introducing a 50 mm x 25 mm cover glass. During the deposition procedure, the bottom of the device was kept on a hot plate at a constant and homogenous temperature (60 ± 3 °C) A metallic reservoir conducts the heat to the cuvette where it takes place the deposition of the pNPs and its temperature was risen slightly above ambient temperature in order to enhance the evaporation rate of the liquid phase but not enough to render IBs inactivation, as proven by the fluorescence images showing bright green fluorescence coming for the GFP-IBs. The open top of the cuvette enables the evaporation of the colloidal suspension and gives also access to a tube leading to the peristaltic pump that allows to control the liquid level of the colloidal suspension and thereby the contact line over the cover glass to be decorated. Thus, the formation of patterns was governed by a programmable peristaltic pump (Watson Marlow 403U/VM2) and its software (FIALab Instruments). This device therefore allows

6

proper temperature control, which is very important for reproducibility, and maintains the intrinsic (non-assisted) solvent evaporation negligible compared to the speed of the pump suction.
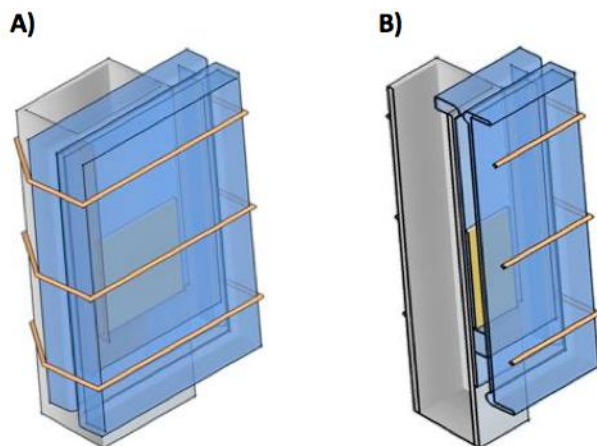

Figure 1. Schematic view of the device designed for an evaporation-assisted pattern deposition. A) Assembled device (the cover glass substrate is marked in yellow, the two planar polystyrene plates in blue, the rectangular metal reservoir in grey and in orange the rubber bands). B) Cross-section of the device.

Surface modification enhancing glass surface-pNPs interactions. The hydrophobicity/hydrophilicity of the glass substrate was optimized to enhance IB deposition. First, the glass slide was cleaned through a series of sonications in ethanol (10 minutes), MilliQ water (10 minutes), and again ethanol (10 minutes). The resulting clean slides, which were dried under a nitrogen flow, were directly used after exposing them to oxygen plasma to develop a hydrophilic character to the surface, or to expose to vapors of hexamethyldisilazane (HMDS, Sigma Aldrich) for 12 hours to obtain a hydrophobic surface. A scheme of the glass silanization process is presented (Figure S1). The most well-defined patterns with narrower deposition areas, i.e. the patterns with the most localized "contact lines" of IBs, were obtained with hydrophobic

7

silanized glasses (Figure S2) due to the stronger interaction of the glass surface with the hydrophobic protein domains of the particles, as it was thoroughly studied before.[47] On the other hand, the deposition area close to the rim was usually broader in the case of hydrophilic substrates. Nevertheless, even if the area was wider, the concentration of IBs was lower than on hydrophobic substrates due to the smaller surface-IBs interaction.

Device calibration protocol for IB deposition. By keeping constant all the intrinsic variables that govern the coffee-drop effect, the evaporation driven deposition rate (number of deposited particles per unit of time) on the three-phase line, i.e. where evaporation and therefore deposition occurs, is constant. Thus, by externally controlling with the pump the rate of movement of the "contact line" (V_{CL}, units of length over time; equivalent to V_V, in units of volume over time; $V_V=V_{CL}\cdot A$, where A is the cross-section of the water-tight vessel) over the substrate, it is possible to control the concentration of deposited material (C_D, number of deposited particles per unit of area). The latter is proportional to the fluorescence intensity of the deposited GFP-IBs (I, in arbitrary units (AU) per pixel; see SI). In this device, the lower the speed of the "contact line" over the sample, the higher the number of deposited particles. In consequence, low speeds are used to deposit high concentrations of IBs, while moderate speeds are used to deposit lower concentrations of particles, and extremely high speeds to obtain areas with practically no particle deposition. The latter conditions were used for separating the areas between deposited IBs (Figure 2).
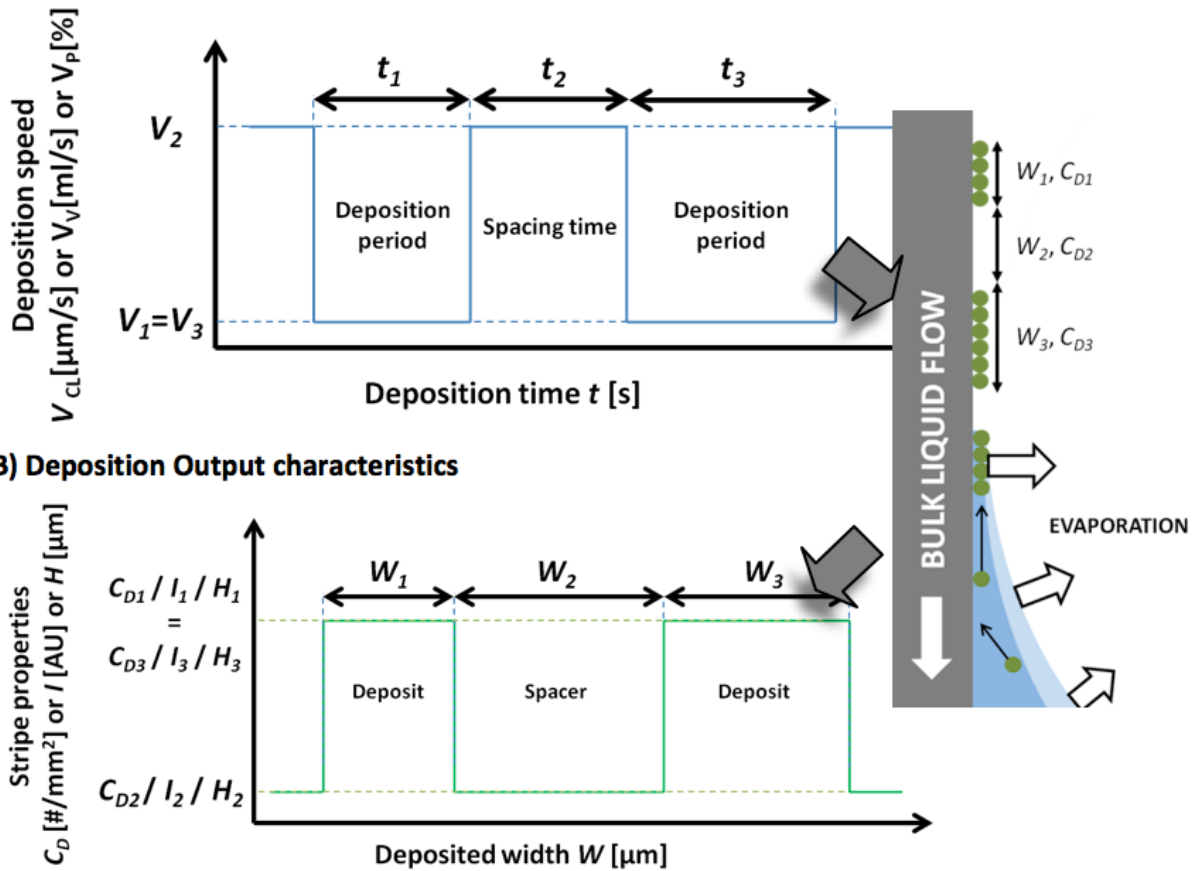
A) Deposition Input parameters

B) Deposition Output characteristics

Figure 2. Scheme of an operational protocol consisting of three consecutive steps (i = 1, 2, 3) with A) deposition input parameters (V_i) and B) output characteristics (C_{Di}, I_i, or H_i), presented on separate plots, resulting in the deposition of three stripes. A constant IB suspension concentration, C_S, is assumed during the whole process.

The device was calibrated to establish how the settings of the pump (input parameters) consisting of the velocity of the "three-phase-line" movement, V_{CL}, (expressed also either as colloidal solution volume pumped per time, V_V, or as % of the maximal pump speed, V_P) and the pumping time, t, influence the deposited pattern features (output characteristics), such as the deposited linewidth, W_n, fluorescence intensity, I_n, height of the deposited materials, H_n, and surface-bound

particle density, C_n. A detailed explanation of input and output parameters can be found in Table S1. A description of calibration experiments with the resulting IB-patterned surfaces derived from the calibration curves can be also found in the SI.

Atomic Force Microscopy (AFM) characterization. A scanning probe microscopy (5500LS SPM AFM; Agilent Technologies) was used to characterize the topography of deposited IB gradients. Samples were imaged using non-contact mode with SSS-NCH tips (Nanosensors).

Optical and fluorescence microscopy. Substrates were routinely observed under an Olympus BX51 microscope equipped with an Olympus DP20 CCD camera, whereas a Leica TCS SP5 AOBS spectral confocal microscope (Leica Microsystems) with a Plan-Apochromat 63x, 1.4 NA lens was used for cell studies.

RESULTS AND DISCUSSION

There is a large demand for methodologies that enable to produce surface-bond gradients of NPs for cell motility studies for applicability in different areas, from tissue engineering to cancer research.[48-52] Although a method to deposit gradients of NPs has been described, it only works with highly homogeneous inorganic NPs.[28-29] It is therefore necessary to develop new strategies to deposit "a-la-carte" concentration gradients of NPs, with controlled widths and slopes of challenging soft particles such as pNPs. Specifically, pNPs such IBs, are produced in living bacteria and show tunable biochemical signals at their surfaces, broader size distributions and lower homogeneity than engineered inorganic NPs.[1, 3, 5, 47] Here we present a device that works with a protocol that is highly versatile, reproducible, does not include masks nor surface

functionalizations, and allows an external control leading to surface-bond gradients of pNPs with controlled characteristics.

Generation of gradients by an evolutionary algorithm

There are numerous factors that influence gradient generation, i.e. the profile of the deposited patterns, which are difficult to control, especially if colloidal suspensions of biologically produced NPs, like IBs, which have higher heterogeneity than synthetic engineered NPs. To overcome this inconvenience, an "evolutionary algorithm" was developed and implemented to optimise the pump settings (input parameters) and to obtain a given gradient deposition of IBs with controlled output characteristics. Evolutionary algorithms are iterative and nature-inspired techniques used to search the space of alternative solutions in order to identify the best ones.[53-54] They are often used in cases of high complexity, where the initial set of conditions (genotype) influences the final outcome (phenotype). The algorithm consists of an initial step (1), in which a number (population) of genotypes (individuals) are generated (first generation). Then, occurs an evaluation step (2) consisting of calculating the fitness function for each individual phenotype. The next step is the selection step (3), in which the best-fitting individuals are chosen (parents). Then, the proliferation step (4) takes place, in which the next generation of genotypes are generated through breeding (mixing of parental genes), mutation (random parameter generation), or a combination of both processes. The newly obtained population is sent to the evaluation step and the algorithm iterates. The algorithm repeats until a limit of time, a certain iteration number, or a sufficient fitness function value are achieved. In our case, the genotypes were the pump settings and the phenotypes were the gradient deposits (visualized from the fluorescence patterns) that resulted from each setting. Following this evolutionary algorithm, a schematic pipeline of the gradient protocol

11

optimization is presented (Figure 3). The duration of one iteration of algorithm depends on the number of individual variations in one generation. In our case, with 10 gradients per lot, step #1 absorbed most of the time (setting up device, deposition and retrieving sample) taking ~2hours. Imaging patterns and retrieving profile data in step #2 is accomplished within 30 minutes, and all the remaining steps are completed immediately once the prepared spreadsheet was feeded with the profile data.
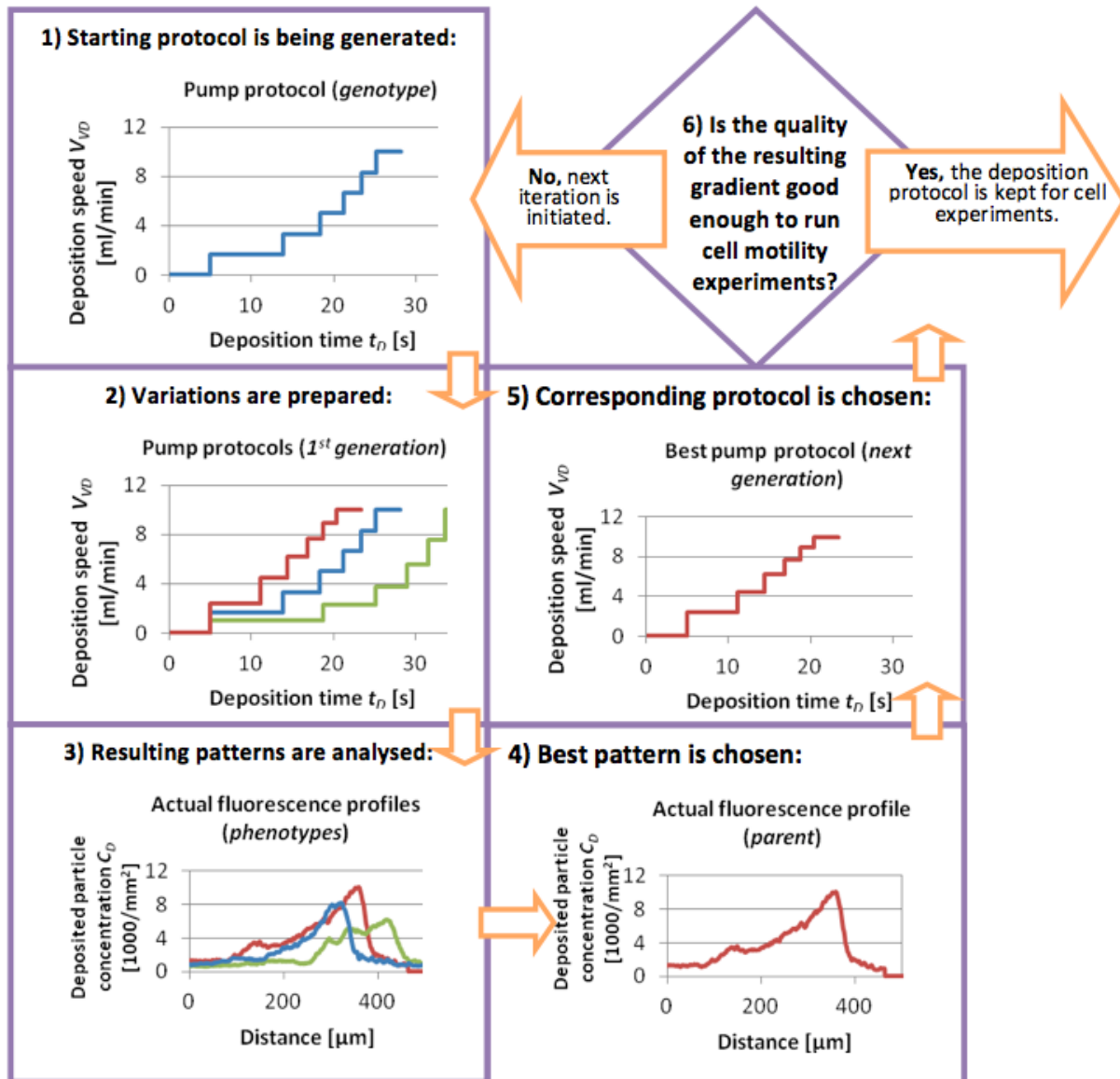
Figure 3. Scheme of the evolutionary algorithm used to develop the protocol for IB gradient deposition. 1) Generation of the starting protocol: 2) variation of the starting protocol; 3) analysis of the resulting patterns; 4) best pattern; 5) best protocol; 6) evaluation of the quality of the result and decide if following with the iteration or keeping the protocol for cell experiments.

In our case, the starting input was one pump-operating protocol (genotype) that consisted of series of different deposition steps using different pump speeds and deposition times. From this starting point, variations of the initial protocol were made, changing slightly each step (time span and/or pump speed). These variations were introduced in a well-defined and controlled manner (a mutation approach was applied within a given threshold). This set of protocols defined the first generation. Subsequently, all protocols were executed and the resulting IB deposition gradients (phenotypes) were assessed by observing the attained gradients through the fluorescent profiles. The evaluation step was based on the control of gradient quality and resulted in numerical values, G, that enabled a quantitative comparison between various deposits, as described in the SI. From all the resulting deposits, the result that best fulfilled the requirements in terms of desired widths and slopes was chosen. If this gradient was the desired one, the protocol was used for preparing IB gradients on surfaces. However, if the result was not satisfactory, the protocol was used as an input to the next iteration of the algorithm (next generation). This process was repeated until the desired gradient was attained. Using this approach, if some imperfections are localized in one part of the resulting deposit, the corresponding part of the protocol can be manually substituted by another protocol that is more adequate for this particular zone (breeding). This possibility gives versatility and robustness to the strategy and allows a successfully optimization of the protocol for the deposition of surface-bound IB gradients.

As an example, an IB deposition protocol that required three iterations (~10 protocols each) to obtain the satisfactory gradient is presented on Figures 4 and 5. Fluorescence images of these three generations are shown (Figure 4) as well as the profiles of particle density, based on the fluorescence intensity measurements of these three generations (Figure 5).
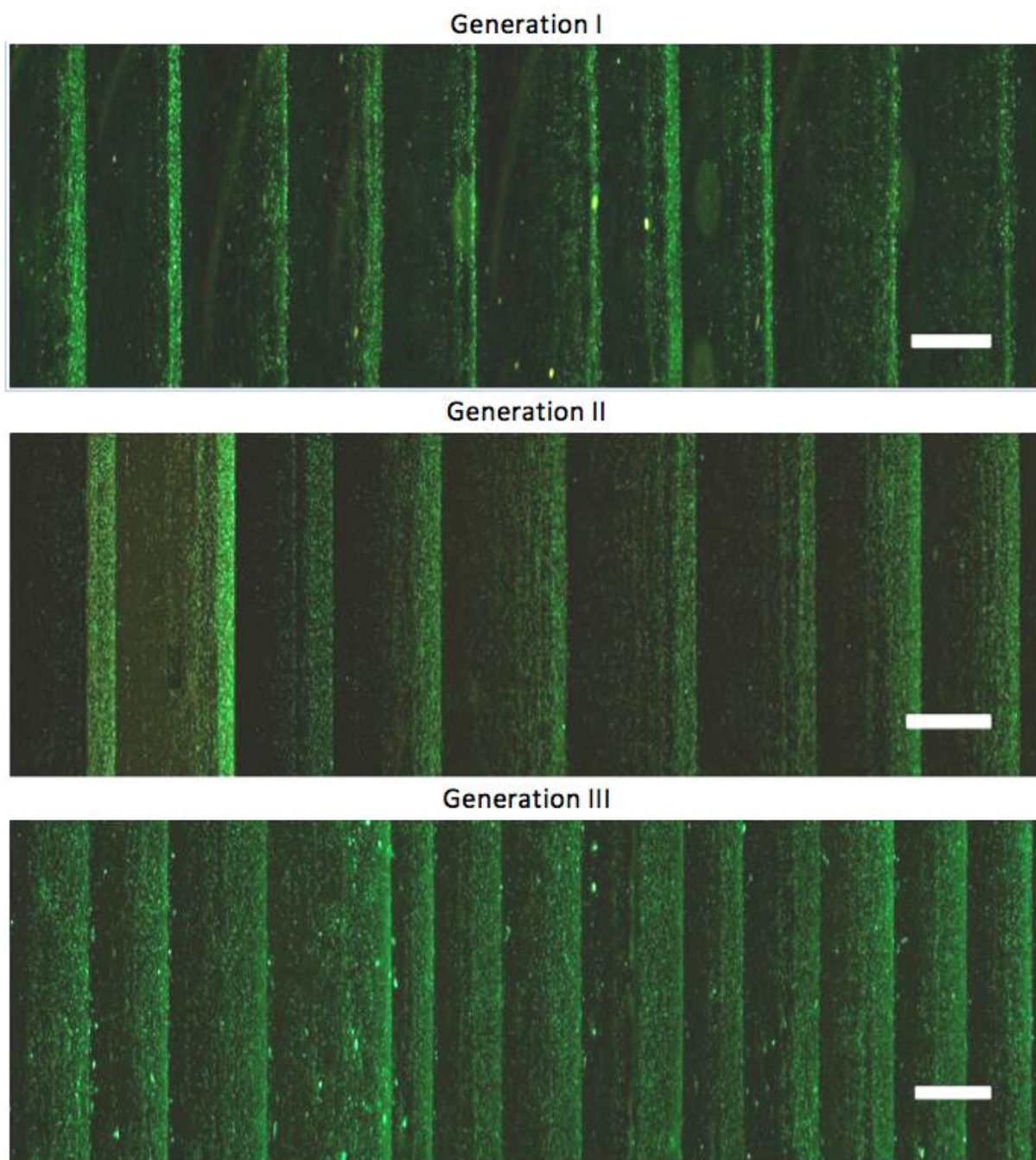
Generation I

Generation II

Generation III

Figure 4. Mosaic of fluorescence microscopy images of the ~10 different resulting patterns (phenotypes) used to obtain the satisfactory gradient. Scale bar = 500 μm.
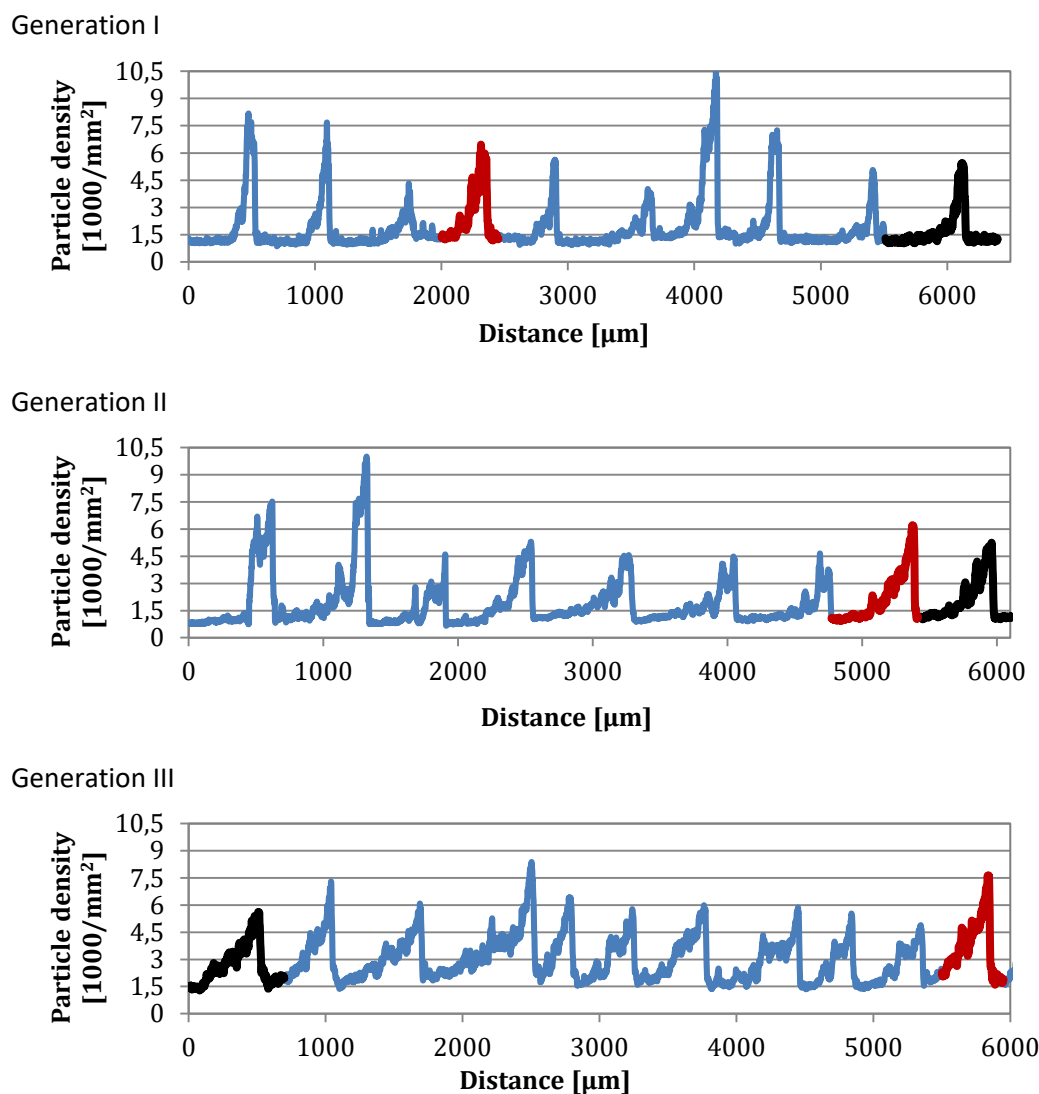
Generation I

Generation II

Generation III

Figure 5. Profiles of gradients of generations I, II, and III. The protocols corresponding to the black profiles were used as "initiator" pump settings, while the profiles marked in red gave the lowest value of the shape descriptor, G, in the series (see SI); i.e., they are the profiles of each generation that best fit the requirements of the desired pattern. Protocols corresponding to red profiles were the "initiator" protocols of the next generation until the desired pattern was obtained.

Production and characterization of surface-bound pNP gradients

Using the previously described device, a protocol for IB gradient deposition was optimized by implementing an evolutionary algorithm. The obtained gradients showed linear changes of NP concentration over broad areas of approximately 500 μm, which could cover both hydrophilic and hydrophobic surfaces of large dimensions (~10 cm^2). As an example of its versatility, the protocol was used to form an array of two dimensional gradients by depositing series of gradients of GFP-derived IBs deposited on a silanized cover glass in two perpendicular directions. The resulting patterns were imaged by optical and fluorescence microscopy. Thus, fluorescence profiles of the gradients were obtained (Figure 6), which demonstrate the successful patterning of the substrates.
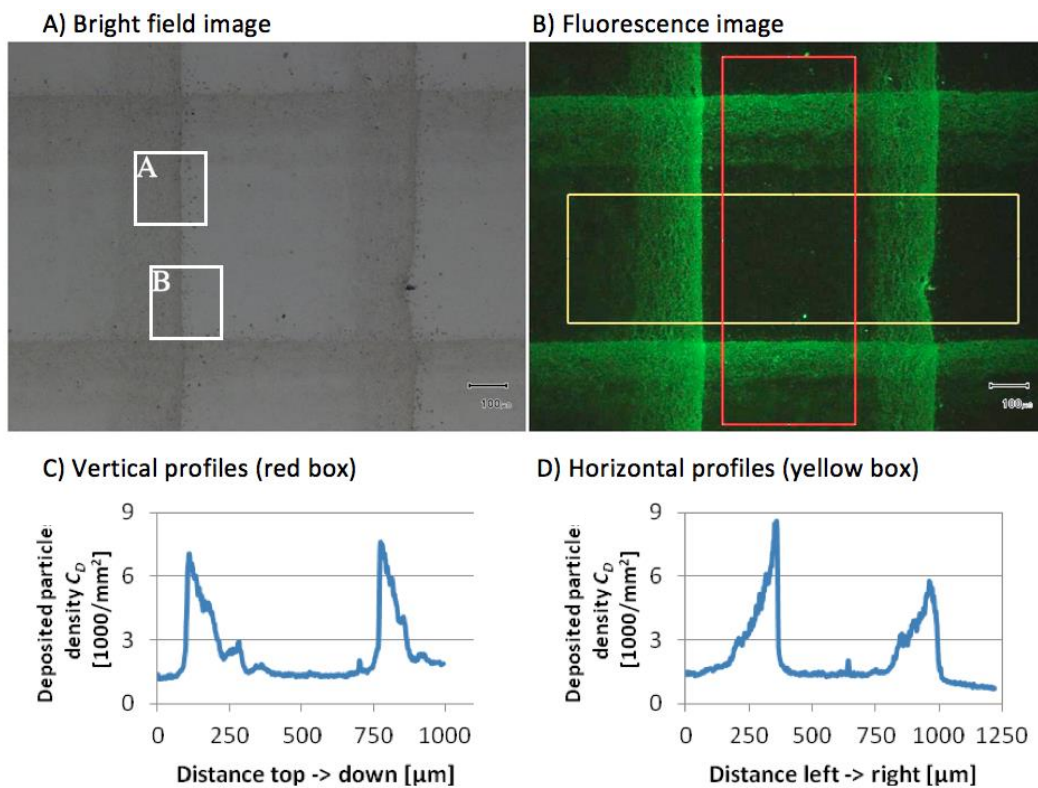

A) Bright field image B) Fluorescence image

C) Vertical profiles (red box) D) Horizontal profiles (yellow box)

Figure 6. Array of two dimensional gradients of GFP-derived IBs deposited on a silanized cover glass. A) Bright field image in which white boxes depict the areas that were characterized by AFM (Figure 5). B) Fluorescence image in which red and yellow boxes are depicting the areas used to prepare vertical and horizontal fluorescence profiles presented in C) and D), respectively.

Moreover, AFM topography profiles and phase contrast maps (Figure 7) were obtained from the areas marked in white in Figure 6A. Deposits are easily distinguishable from the underlying glass substrates in both topography and phase contrast modes, which indicates that the layer of IBs have a different morphology as well as mechanical properties than the substrate material.
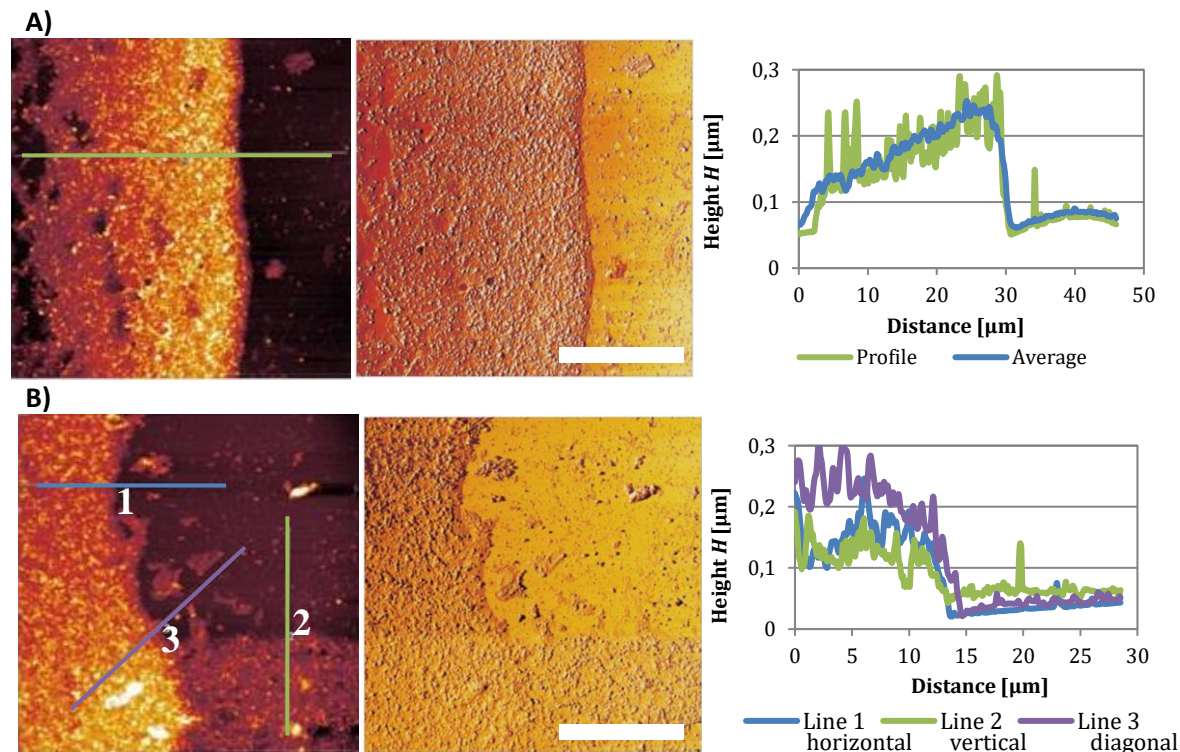

18

Figure 7. AFM images (left: topography contrast, right: phase contrast) and height profiles of single and complex gradients. Profiles correspond to lines marked in the topography images. A) corresponds to the A white square and B) to the B white square marked in Figure 6A. White bars indicate 20μm.

Two profiles of gradient topography are presented (Figure 7A, right). The green one corresponds to the profile of the marked line, while the blue one is an averaged profile of the whole image. Figure 7 proves that we have managed to deposit gradients of density (number of particles per unit area). The green profile contains peaks that can be assigned to the presence of individual IB particles that appear all over the deposited area. Even for low concentrations of particles there are high peaks corresponding to IB's inherit size. On the other hand, the blue profile is smoother, as it averages the heights along a large area and since the number of particles grows towards the edge of a gradient, so is the average height. Another important conclusion is that even in areas with very densely packed IBs, these pNPs did not form a multilayer, as the height is within the range of a single IB diameter. Moreover, horizontal (blue), vertical (green), and diagonal (purple) profiles derived from the perpendicular intersection of two gradient patterns are shown (Figure 7B, right). As expected, the horizontal and vertical patterns are very similar, as they are produced by the same protocol. The purple profile therefore shows a higher topography, because it is the superposition of two IB deposited and it therefore contains more pNPs.

CONCLUSIONS

A method to produce pNP gradients in a controlled and reproducible manner based on the coffee-drop effect is presented. This method can be readily applied to a flat surface, i.e. it does not require masks, stamps, replicas, surface functionalizations, or any other type of labelling. The evaporation-assisted methodology here described was applied in a custom device designed for this purpose using an evolutionary algorithm, that enabled the preparation of striped pNP patterns with gradients of controlled widths and heights. Thus, fully customizable patterns with broad pNP stripes of approximately 500 μm covering large areas ($\sim$10 cm^2) could be obtained in a fast and cost-effective manner. In conclusion, the developed method opens the possibility to decorate surfaces "a-la-carte" with pNPs for different applications such as cell motility studies. Such patterns could be used for both restricting and guiding cell movement as will be presented in a forthcoming publication.

ASSOCIATED CONTENT

Supporting Information. Surface preparation and its impact on deposits, calibration details concerning deposited stripe width and concentration, description of the evaluation step implemented in the evolutionary algorithm.

AUTHOR INFORMATION

Address correspondence to: vecianaj@icmab.es, iratera@icmab.es

"Dynamic Biomimetics for Cancer Immunotherapy" in collaboration with the Max Planck for Medical Research (Heidelberg, Germany).

REFERENCES

(1) Rinas, U.; Garcia-Fruitós, E.; Corchero, J. L.; Vázquez, E.; Seras-Franzoso, J.; Villaverde, A. Bacterial Inclusion Bodies: Discovering Their Better Half *Trends Biochem. Sci.* **2017**, *42*, 727-737.

(2) Vázquez, E.; Corchero, J. L.; Burgueño, J. F.; Seras-Franzoso, J.; Kosoy, A.; Bosser, R.; Mendoza, R.; Martínez-Láinez, J. M.; Rinas, U.; Fernández, E.; Ruiz-Avila, L.; García-Fruitós, E.; Villaverde, A. Functional Inclusion Bodies Produced in Bacteria as Naturally Occurring Nanopills for Advanced Cell Therapies *Adv. Mater.* **2012**, *24*, 1742-1747.

(3) García-Fruitós, E. Inclusion Bodies: A New Concept *Microb. Cell Fact.* **2010**, *9*, 1-3.

(4) Torrealba, D.; Parra, D.; Seras-Franzoso, J.; Vallejos-Vidal, E.; Yero, D.; Gibert, I.; Villaverde, A.; Garcia-Fruitós, E.; Roher, N. Nanostructured Recombinant Cytokines: A Highly Stable Alternative to Short-Lived Prophylactics *Biomaterials* **2016**, *107*, 102-114.

(5) Villaverde, A.; Corchero, J. L.; Seras-Franzoso, J.; Garcia-Fruitós, E. Functional Protein Aggregates: Just the Tip of the Iceberg *Nanomedicine (Lond.)* **2015**, *10*, 2881-2891.

(6) Seras-Franzoso, J.; Tatkiewicz, W. I.; Vazquez, E.; García-Fruitós, E.; Ratera, I.; Veciana, J.; Villaverde, A. Integrating Mechanical and Biological Control of Cell Proliferation through Bioinspired Multieffector Materials *Nanomedicine (Lond.)* **2015**, *10*, 873-891.

(7) Céspedes, M. V.; Fernández, Y.; Unzueta, U.; Mendoza, R.; Seras-Franzoso, J.; Sánchez-Chardi, A.; Álamo, P.; Toledo-Rubio, V.; Ferrer-Miralles, N.; Vázquez, E.; Jr., S. S.; Abasolo, I.;

Corchero, J. L.; Mangues, R.; Villaverde, A. Bacterial Mimetics of Endocrine Secretory Granules as Immobilized in Vivo Depots for Functional Protein Drugs *Sci. Rep.* **2016**, *6*, 1-10.

(8) Unzueta, U.; Seras-Franzoso, J.; Céspedes, M. V.; Saccardo, P.; Cortés, F.; Rueda, F.; Garcia-Fruitós, E.; Ferrer-Miralles, N.; Mangues, R.; Vázquez, E.; Villaverde, A. Engineering Tumor Cell Targeting in Nanoscale Amyloidal Materials *Nanotechnology* **2017**, *28*, 1-10.

(9) Seras-Franzoso, J.; Sánchez-Chardi, A.; Garcia-Fruitós, E.; Vázquez, E.; Villaverde, A. Cellular Uptake and Intracellular Fate of Protein Releasing Bacterial Amyloids in Mammalian Cells *Soft Matter* **2016**, *12*, 3451-3460.

(10) Tatkiewicz, W. I.; Seras-Franzoso, J.; García-Fruitós, E.; Vazquez, E.; Ventosa, N.; Peebo, K.; Ratera, I.; Villaverde, A.; Veciana, J. Two-Dimensional Microscale Engineering of Protein-Based Nanoparticles for Cell Guidance *ACS Nano* **2013**, *7*, 4774-4784.

(11) Petrie, R. J.; Doyle, A. D.; Yamada, K. M. Random Versus Directionally Persistent Cell Migration *Nat. Rev. Mol. Cell Biol.* **2009**, *10*, 538-549.

(12) Geiger, B.; Spatz, J. P.; Bershadsky, A. D. Environmental Sensing through Focal Adhesions *Nat. Rev. Mol. Cell Biol.* **2009**, *10*, 21-33.

(13) Wu, A.; Loutherback, K.; Lambert, G.; Estévez-Salmerón, L.; Tlsty, T. D.; Austin, R. H.; Sturm, J. C. Cell Motility and Drug Gradients in the Emergence of Resistance to Chemotherapy *Proc. Natl. Acad. Sci. U.S.A* **2013**, *110*, 16103-16108.

(14) Moissoglu, K.; Majumdar, R.; Parent, C. A. Cell Migration: Sinking in a Gradient *Curr. Biol.* **2014**, *24*, R23-R25.

(15) Kölsch, V.; Charest, P. G.; Firtel, R. A. The Regulation of Cell Motility and Chemotaxis by Phospholipid Signaling *J. Cell Sci.* **2008**, *121*, 551-559.

(16) Kim, H. S.; Chen, Y.-C.; Nör, F.; Warner, K. A.; Andrews, A.; Wagner, V. P.; Zhang, Z.; Zhang, Z.; Martins, M. D.; Pearson, A. T.; Yoon, E.; Nör, J. E. Endothelial-Derived Interleukin-6 Induces Cancer Stem Cell Motility by Generating a Chemotactic Gradient Towards Blood Vessels *Oncotarget* **2017**, *8*, 100339-100352.

(17) Han, W.; Lin, Z. Learning from "Coffee Rings": Ordered Structures Enabled by Controlled Evaporative Self-Assembly *Angew. Chem. Int. Ed.* **2012**, *51*, 1534-1546.

(18) Guasch, J.; Diemer, J.; Riahinezhad, H.; Neubauer, S.; Kessler, H.; Spatz, J. P. Synthesis of Binary Nanopatterns on Hydrogels for Initiating Cellular Responses *Chem. Mater.* **2016**, *28*, 1806-1815.

(19) Lohmueller, T.; Aydin, D.; Schwieder, M.; Morhard, C.; Louban, I.; Pacholski, C.; Spatz, J. P. Nanopatterning by Block Copolymer Micelle Nanolithography and Bioinspired Applications *Biointerphases* **2011**, *6*, MR1-MR12.

(20) Aydin, D.; Louban, I.; Perschmann, N.; Bluemmel, J.; Lohmueller, T.; Cavalcanti-Adam, E. A.; Haas, T. L.; Walczak, H.; Kessler, H.; Fiammengo, R.; Spatz, J. P. Polymeric Substrates with Tunable Elasticity and Nanoscopically Controlled Biomolecule Presentation *Langmuir* **2010**, *26*, 15472-15480.

(21) Guasch, J.; Muth, C. A.; Diemer, J.; Riahinezhad, H.; Spatz, J. P. Integrin-Assisted T-Cell Activation on Nanostructured Hydrogels *Nano Lett.* **2017**, *17*, 6110-6116.

(22) Pallarola, D.; Bochen, A.; Guglielmotti, V.; Oswald, T. A.; Kessler, H.; Spatz, J. P. Highly Ordered Gold Nanopatterned Indium Tin Oxide Electrodes for Simultaneous Optical and Electrochemical Probing Cell Interactions *Anal. Chem.* **2017**, *89*, 10054-10062.

(23) Rechenmacher, F.; Neubauer, S.; Mas-Moruno, C.; Dorfner, P. M.; Polleux, J.; Guasch, J.; Conings, B.; Boyen, H.-G.; Bochen, A.; Sobahi, T. R.; Burgkart, R.; Spatz, J. P.; Fässler, R.;

Kessler, H. A Molecular Toolkit to Functionalize Ti-Based Biomaterials That Selectively Control Integrin-Mediated Cell Adhesion *Chem. Eur. J.* **2013**, *19*, 9218-9223.

(24) Layani, M.; Gruchko, M.; Milo, O.; Balberg, I.; Azulay, D.; Magdassi, S. Transparent Conductive Coatings by Printing Coffee Ring Arrays Obtained at Room Temperature *ACS Nano* **2009**, *3*, 3537-3542.

(25) Higashitani, K.; McNamee, C. E.; Nakayama, M. Formation of Large-Scale Flexible Transparent Conductive Films Using Evaporative Migration Characteristics of Au Nanoparticles *Langmuir* **2011**, *27*, 2080-2083.

(26) Fan, J. A.; Bao, K.; Sun, L.; Bao, J.; Manoharan, V. N.; Nordlander, P.; Capasso, F. Plasmonic Mode Engineering with Templated Self-Assembled Nanoclusters *Nano Lett.* **2012**, *12*, 5318-5324.

(27) Genzer, J. Surface-Bound Gradients for Studies of Soft Materials Behavior *Annu. Rev. Mater. Sci.* **2012**, *42*, 435-468.

(28) Arnold, M.; Hirschfeld-Warneken, V. C.; Lohmüller, T.; Heil, P.; Blümmel, J.; Cavalcanti-Adam, E. A.; López-García, M.; Walther, P.; Kessler, H.; Geiger, B.; Spatz, J. P. Induction of Cell Polarization and Migration by a Gradient of Nanoscale Variations in Adhesive Ligand Spacing *Nano Lett.* **2008**, *8*, 2063-2069.

(29) Jakubick, V. C.; Arnold, M.; Cavalcanti-Adam, A.; López-García, M.; Kessler, H.; Spatz, J. P. Cell Adhesion and Polarisation on Molecularly Defined Spacing Gradient Surfaces of Cyclic Rgdfk Peptide Patches *Eur. J. Cell Biol.* **2008**, *87*, 743-750.

(30) Byun, M.; Han, W.; Li, B.; Xin, X.; Lin, Z. An Unconventional Route to Hierarchically Ordered Block Copolymers on a Gradient Patterned Surface through Controlled Evaporative Self-Assembly *Angew. Chem. Int. Ed.* **2013**, *52*, 1122-1127.

(31) Shen, X.; Ho, C.-M.; Wong, T.-S. Minimal Size of Coffee Ring Structure *J. Phys. Chem. B* **2010**, *114*, 5269-5274.

(32) Yin, Y.; Lu, Y.; Gates, B.; Xia, Y. Template-Assisted Self-Assembly: A Practical Route to Complex Aggregates of Monodispersed Colloids with Well-Defined Sizes, Shapes, and Structures *J. Am. Chem. Soc.* **2001**, *123*, 8718-8729.

(33) Xia, D.; Biswas, A.; Li, D.; Brueck, S. R. J. Directed Self-Assembly of Silica Nanoparticles into Nanometer-Scale Patterned Surfaces Using Spin-Coating *Adv. Mater.* **2004**, *16*, 1427-1432.

(34) Celio, H.; Barton, E.; Stevenson, K. J. Patterned Assembly of Colloidal Particles by Confined Dewetting Lithography *Langmuir* **2006**, *22*, 11426-11435.

(35) Harris, D. J.; Hu, H.; Conrad, J. C.; Lewis, J. A. Patterning Colloidal Films Via Evaporative Lithography *Phys. Rev. Lett.* **2007**, *98*, 148301.

(36) Masuda, Y.; Itoh, T.; Koumoto, K. Self-Assembly Patterning of Silica Colloidal Crystals *Langmuir* **2005**, *21*, 4478-4481.

(37) Choi, Y.-J.; Luo, T.-J. M. Self-Assembly of Silver−Aminosilica Nanocomposites through Silver Nanoparticle Fusion on Hydrophobic Surfaces *ACS Appl. Mater. Interfaces* **2009**, *1*, 2778-2784.

(38) Fan, F.; Stebe, K. J. Assembly of Colloidal Particles by Evaporation on Surfaces with Patterned Hydrophobicity *Langmuir* **2004**, *20*, 3062-3067.

(39) Kraus, T.; Malaquin, L.; Schmid, H.; Riess, W.; Spencer, N. D.; Wolf, H. Nanoparticle Printing with Single-Particle Resolution *Nat. Nanotechnol.* **2007**, *2*, 570-576.

(40) Kim, H. S.; Lee, C. H.; Sudeep, P. K.; Emrick, T.; Crosby, A. J. Nanoparticle Stripes, Grids, and Ribbons Produced by Flow Coating *Adv. Mater.* **2010**, *41*, 4600-4604.

(41) Mino, Y.; Watanabe, S.; Miyahara, M. T. Colloidal Stripe Pattern with Controlled Periodicity by Convective Self-Assembly with Liquid-Level Manipulation *ACS Appl. Mater. Interfaces* **2012**, *4*, 3184-3190.

(42) Watanabe, S.; Miyahara, M. T. Particulate Pattern Formation and Its Morphology Control by Convective Self-Assembly *Adv. Powder Technol.* **2013**, *24*, 897-907.

(43) Hanafusa, T.; Mino, Y.; Satoshi Watanabe; Miyahara, M. T. Controlling Self-Assembled Structure of Au Nanoparticles by Convective Self-Assembly with Liquid-Level Manipulation *Adv. Powder Technol.* **2014**, *25*, 811-815.

(44) Mino, Y.; Watanabe, S.; Miyahara, M. T. Fabrication of Colloidal Grid Network by Two-Step Convective Self-Assembly *Langmuir* **2011**, *27*, 5290-5295.

(45) Watanabe, S.; Mino, Y.; Ichikawa, Y.; Miyahara, M. T. Spontaneous Formation of Cluster Array of Gold Particles by Convective Self-Assembly *Langmuir* **2012**, *28*, 12982.

(46) Tsai, H.-Y.; Vats, K.; Yates, M. Z.; Benoit, D. S. W. Two-Dimensional Patterns of Poly(N-Isopropylacrylamide) Microgels to Spatially Control Fibroblast Adhesion and Temperature-Responsive Detachment *Langmuir* **2013**, *29*, 12183-12193.

(47) Díez-Gil, C.; Krabbenborg, S.; García-Fruitós, E.; Vazquez, E.; Rodríguez-Carmona, E.; Ratera, I.; Ventosa, N.; Seras-Franzoso, J.; Cano-Garrido, O.; Ferrer-Miralles, N.; Villaverde, A.; Veciana, J. The Nanoscale Properties of Bacterial Inclusion Bodies and Their Effect on Mammalian Cell Proliferation *Biomaterials* **2010**, *31*, 5805-5812.

(48) Lutolf, M. P.; Hubbell, J. A. Synthetic Biomaterials as Instructive Extracellular Microenvironments for Morphogenesis in Tissue Engineering *Nat. Biotechnol.* **2005**, *23*, 47-55.

(49) Makris, E. A.; Gomoll, A. H.; Malizos, K. N.; Hu, J. C.; Athanasiou, K. A. Repair and Tissue Engineering Techniques for Articular Cartilage *Nat. Rev. Rheumatol.* **2015**, *11*, 21-34.

(50) Madsen, C. D.; Hooper, S.; Tozluoglu, M.; Bruckbauer, A.; Fletcher, G.; Erler, J. T.; Bates, P. A.; Thompson, B.; Sahai, E. Stripak Components Determine Mode of Cancer Cell Migration and Metastasis *Nat. Cell Biol.* **2015**, *17*, 68-80.

(51) Sadok, A.; McCarthy, A.; Caldwell, J.; Collins, I.; Garrett, M. D.; Yeo, M.; Hooper, S.; Sahai, E.; Kuemper, S.; Mardakheh, F. K.; Mars, C. J. Rho Kinase Inhibitors Block Melanoma Cell Migration and Inhibit Metastasis *Cancer Res.* **2015**, *75*, 2272-2284.

(52) Guasch, J.; Conings, B.; Neubauer, S.; Rechenmacher, F.; Ende, K.; Rolli, C. G.; Kappel, C.; Schaufler, V.; Micoulet, A.; Kessler, H.; Boyen, H.-G.; Cavalcanti-Adam, E. A.; Spatz, J. P. Segregation Versus Colocalization: Orthogonally Functionalized Binary Micropatterned Substrates Regulate the Molecular Distribution in Focal Adhesions *Adv. Mater.* **2015**, *27*, 3737–3747.

(53) Whitley, D. An Overview of Evolutionary Algorithms: Practical Issues and Common Pitfalls *Inf. Softw. Technol.* **2001**, *43*, 817-831.

(54) Hibbert, D. B. Genetic Algorithms in Chemistry *Chemom. Intell. Lab. Syst.* **1997**, *19*, 277-283.

TABLE OF CONTENTS

Evaporation-assisted deposition of protein nanoparticles